Directed Photocurrents in Nanostructured TiO_2/SnO_2 Heterojunction Diodes

Boris Levy* and Wang Liu

Department of Chemistry, Boston University, Boston, Massachusetts 02215

Scott E. Gilbert*

Institute of Experimental Physics, Swiss Federal Institute of Technology, CH-1015 Lausanne, Switzerland

Received: July 15, 1996; In Final Form: November 19, 1996[⊗]

Time-resolved photocharge (TRPC) measurements are applied for the first time to demonstrate the presence of a contact potential between lightly sintered colloidal nanocrystalline TiO_2 films deposited on transparent highly conductive tin oxide films degenerately doped with fluorine, SnO_2(F). By virtue of its contactless nature and absence of an externally applied field, TRPC has previously been demonstrated to possess the capability to directly probe the electric field in semiconductor heterojunction particulate materials without the complications and ambiguities encountered with many other measurement techniques. Using TRPC, vectorial directions of photoelectron currents in glass/SnO_2(F)/TiO_2 samples, as determined by signal polarity, are found to be dependent on their orientation with respect to the incident photon flux (*i.e.*, negative polarity for exposure through the glass; positive polarity for exposure directly on the TiO_2). This implies that photoelectrons always flow toward the SnO_2(F)/TiO_2 interface. In a control experiment, in the absence of SnO_2(F), with the nanoporous TiO_2 deposited directly onto the glass, the TRPC signal polarity is negative regardless of sample orientation. These results suggest the presence of a contact potential at the SnO_2(F)/TiO_2 interface, with downward band bending from the TiO_2 to the SnO_2(F). The implications of these results in photovoltaic applications are discussed.

Introduction

Nanocrystalline and nanoporous semiconducting oxide thin films are rapidly coming into the forefront as a new class of materials for catalysis and photocatalysis. In this connection, the past decade has witnessed the development of several new types of electrochemical and chemicoelectronic devices based on nanocrystalline colloidal TiO_2 films, such as the Grätzel liquid junction photovoltaic cell,[1] electrochemical electrochromic devices,[2] and solid state sensors.[3] The aforementioned examples are distinguished from their compact-film counterparts by their superior performance. The properties afforded these devices are derived primarily from the enormous surface area of the nanocrystalline films—up by a factor of ∼1000 or more from compact thin films. The electronic properties of these materials are believed to be derived from the largely enhanced surface area. The role of localized states in the electronic conductivity is greatly exaggerated in comparison to compact films. In addition, because of the extremely small size of the individual particles that comprise the film structure (typically 1−50 nm), some size quantization effects are emphasized, particularly confinement of photogenerated charge carriers in the particles.[4,5]

Due to the complex morphology of nanocrystalline oxide films, attempts to model underlying electronic structure have been impeded. Nor is it possible to use standard models based on compact materials to describe the heterojunctions formed between these and other materials.[6] The conduction mechanism of charge carriers in these films is not well understood. However, this difficulty has been circumvented to some extent by the advancement of simple models that explain experimentally observed results with relative success. Specifically, transient electrochemically derived photocurrents have been simulated using a trap filling and emptying model based on Shockley−Read−Hall trap kinetics.[7] It was shown in this model that deep traps can control the rise and decay time constants of the transients and that a wide distribution of traps was needed in the simulation to adequately describe the experimental curves. Moreover, the photoelectrochemical behavior of colloidal TiO_2 (anatase) film electrodes has been modeled on the basis of carrier diffusion through the film, from point of generation to the back contact.[8]

Convincing experimental evidence indicating that traps are operative in colloidal films includes measurements of slow nonexponential photocurrent decay which depends on the applied reverse bias.[9] Several other related studies of note are cited here.[10−16] Conduction by extended states obtained by interparticle contact presumably plays a role; however, the relative importance of the extended over localized state conduction is not known and may depend on the conditions under which the films are employed.

The nature of the heterojunction formation between nanocrystalline nanoporous films and other materials has not been thoroughly investigated, particularly for the formation of contact potentials. In this article, we present results that directly reveal the existence of a built-in contact potential at the SnO_2(F)/TiO_2 heterojunction by observation of vectorial transient photocurrents that are detected by means of time-resolved photocharge (TRPC) measurements.[17] Here the SnO_2(F) is a compact transparent film degenerately doped with fluorine coated on glass, used to form the back electrode contact of the lightly sintered, ∼8 μm thick, nanoporous TiO_2 colloidal film. Scanning electron micrographs of cross sections of SnO_2(F)/TiO_2 coatings, prepared by a similar procedure to the experimental coatings of the present investigation, suggest a somewhat more compact TiO_2 deposit in the region immediately adjacent to the interface with SnO_2(F), as compared to the more open nanoporous structure in the remaining portion of the TiO_2 coating.[1] However, detailed knowledge of the precise composition and structure of the interfacial region is lacking, and consequently

[⊗] Abstract published in *Advance ACS Abstracts,* February 15, 1997.

S1089-5647(96)02105-0 CCC: $14.00

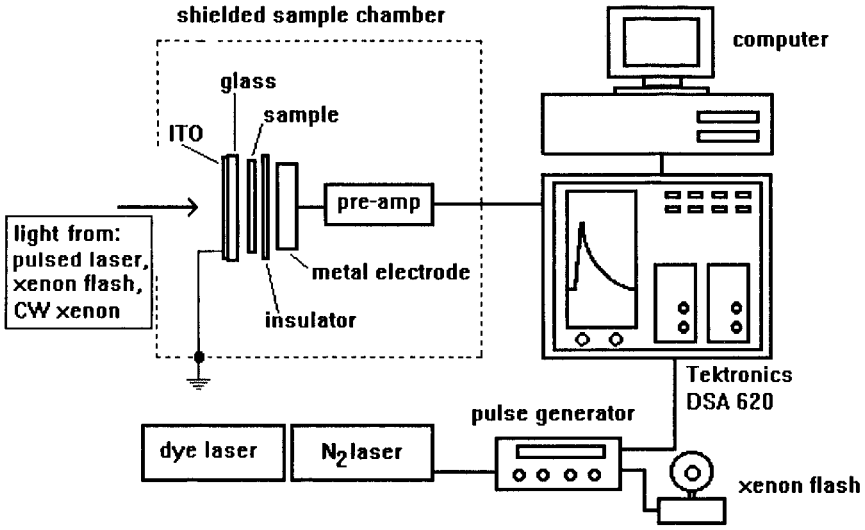

Figure 1. Schematic diagram of TRPC photocharge apparatus.

any influence on photoinduced currents is presently a matter of conjecture. Nonetheless, it seems reasonable to assume that preparative procedures are likely to influence submicron morphology, potential gradients, and consequently the observed photocurrents across the junctions. Resolution of such questions, while worthy of major consideration in future studies, is not the subject of the present paper, which is limited to the study of samples prepared by a somewhat standardized procedure which has evolved for this type of nanoporous coating,[1] as described briefly in the section on *sample preparation*.

In comparing results reported in the present investigation with those of similar systems, it should be kept in mind that we are not employing an electrolyte. Nonetheless, our results with electrolyte free glass/SnO_2(F)/TiO_2 appear to be in essential agreement with other studies utilizing a nonaqueous I_3^-/I^-, electrolyte.[1,2,7,8] This suggests that this electrolyte does not radically alter the potential distribution across the SnO_2(F)/TiO_2 portion of the SnO_2(F)/TiO_2/(I_3^-/I_2, electrolyte) heterojunction, insofar as it might alter the vectorial direction of photoelectron currents, allowing efficient collection by the SnO_2(F) phase.

As discussed by Hodes *et al.*[18] and by Sadeghi *et al.*,[19] photohole and photoelectron acceptors, such as adsorbed H_2O and O_2, may be expected to exert large influences on the magnitudes and in some cases the polarity of photoinduced currents. For this reason, as a followup on work performed at ambient conditions discussed in the present paper, experimentation at more carefully controlled H_2O partial pressures is indicated.

Detailed descriptions of the TRPC measurement, as well as an equivalent circuit analysis have been presented in refs 17 and 19−22, including a description of the calibration of the apparatus for purposes of evaluation of the mean ambipolar charge carrier separation distance (CCSD) and possible perturbations due to heterojunction contacts. A brief description is repeated here, along with a schematic diagram of the apparatus in Figure 1, and equivalent circuit diagrams in the measurement and calibration modes in Figure 2.

The basis for the TRPC measurement rests on the time-resolved charging of the sample cell blocking electrodes (between which the sample is positioned). The capacitive coupling of a transient charge is induced in a photoconductive sample by a laser pulse, and the blocking electrodes are likewise charged by capacitive coupling. The blocking electrodes subsequently discharge through a resistance where the voltage drop is measured and recorded by a transient digitizer (cf. Figures 1 and 2). The system is calibrated by use of a small test capacitance, connected to one of the electrodes, whereby a known charge is injected into the circuit. In this way, a known correspondence is established between the charge and the observed signal, and together with the number of incident quanta and sample absorptivity, the effective charge carrier separation distance (CCSD) between electrons and holes can be calculated.

With reference to Figure 2, it has been shown[17,19−22] that

$$\mathrm{CCSD} = |\mathrm{Vm}|\left(\frac{Va}{Vt}\right)\left(\frac{\epsilon_s}{\epsilon_{ins}}\right)\left(\frac{\dfrac{C}{\mathrm{Ct}+C}}{\dfrac{I}{h\nu}\dfrac{\%A}{100}}\right)d \qquad (1)$$

and for fixed light intensity and constant sample thickness,

$$\mathrm{CCSD} = (\mathrm{const})|\mathrm{Vm}| \qquad (2)$$

In (1) and (2), |Vm| is the magnitude of the maximum TRPC signal amplitude, I the incident laser pulse energy, $h\nu$ the energy per laser photon, % *A* the percent absorption of laser pulse by the sample, and the constant contains experimentally accessible terms or terms that can be reasonably estimated, such as the dielectric constants of the sample, ϵ_s, and the insulating components of the sample cell, ϵ_{ins}, the cell capacitance, *C*; capacitance of test capacitor, Ct, calibration voltages, Va and Vt, and the electrode spacing of the sample cell, *d*. Or from a pragmatic standpoint, the relative values of CCSD or |Vm| may be used to evaluate trends resulting from variations in material parameters.

This can also be seen intuitively by consideration of a basic principle of measurement of charge carrier transport in time-of-flight measurements, as delineated by Tiedje:[23] "... an injected charge inside the (photoconducting) material contributes to the integrated charge flowing in the external circuit in proportion to how far it moves through the sample. That is, if one electron moves halfway across the sample, one-half an electron charge will flow through the external circuit." This same analysis is applicable to TRPC measurements, implying that the magnitude of the TRPC signal amplitude is proportional to the mean charge carrier separation distance, CCSD. Thus, |*Vm*| may be considered to be a photomoment whose magnitude is dependent on the number of photoinduced change carriers and their mean separation distance, CCSD.

The sign of the TRPC response is the resultant of the vectorial photocurrents in the direction perpendicular to the blocking sample cell capacitor parallel plate electrodes. In the absence

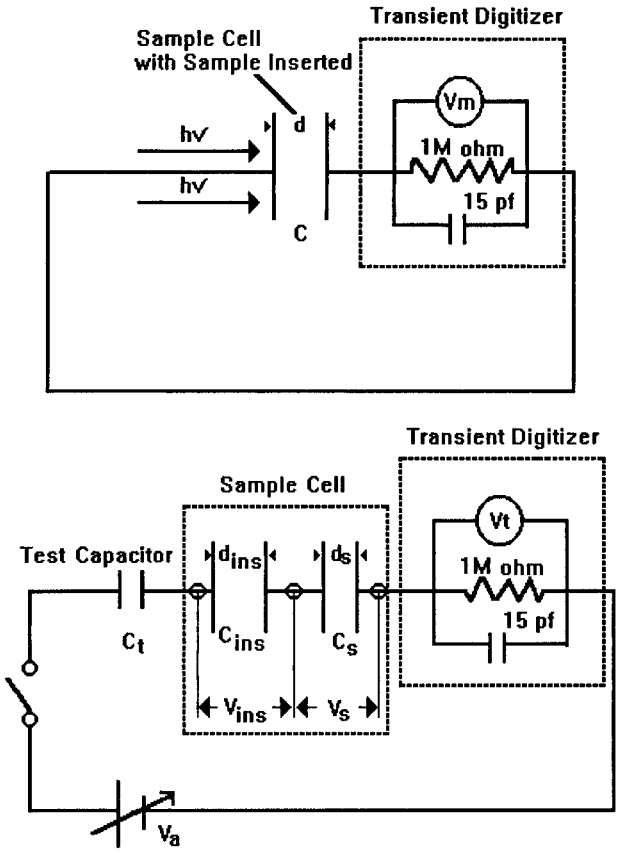

Figure 2. Equivalent circuit diagrams for TRPC determinations: (a, top) measurement mode; (b, bottom) calibration mode for determination of charge carrier separation distance, CCSD.

of space charge fields, the signal depends on inhomogeneously absorbed light and on a difference in charge carrier velocity for the photoelectrons and photoholes and may be considered as equivalent to a time-resolved Dember effect.[17,19−22] Dielectric confinement effects can influence the location of the region of highest light absorption and thereby the sign of the TRPC response.[24,25]

Depletion layers, inversion layers, and surface contact potentials also influence the magnitude and direction of photoinduced currents.[17,19−22,26,27] The polarity convention of the TRPC signal for *n-type* photoconductors is the following: a negative voltage results from vectorial electron transport in the same direction as that of the photon flux from the laser pulse, and a positive signal originates when electron transport is opposed to the photon flux. Figure 3a shows the situation for strongly absorbed light, where electron−hole pairs are generated at the front of the film, and electrons diffuse toward the interior of the film. For weakly absorbed light, as shown in Figure 3b, the highest concentration of electron−hole pairs are generated at the back of the film, and electrons diffuse toward the front, opposite to the photon flux. This is due to dielectric confinement effects causing constructive interference of the incident and reflected light at the inside back surface of the sintered particles. The result is higher light intensity at the inside back surface, as compared to the front surface of an individual particle, or aggregate unit acting as larger light-absorbing entity.[24,25] The resulting TRPC signals, equivalent in these examples to Dember signals, but having opposite polarities with respect to the photon flux, are shown for each case.

The wavelength-dependent onset of TRPC polarity reversals have been demonstrated to vary with (i) sample thickness, (ii) absorption coefficient of the sample at the excitation wavelength, (iii) refractive indexes of the photoconducting sample and that

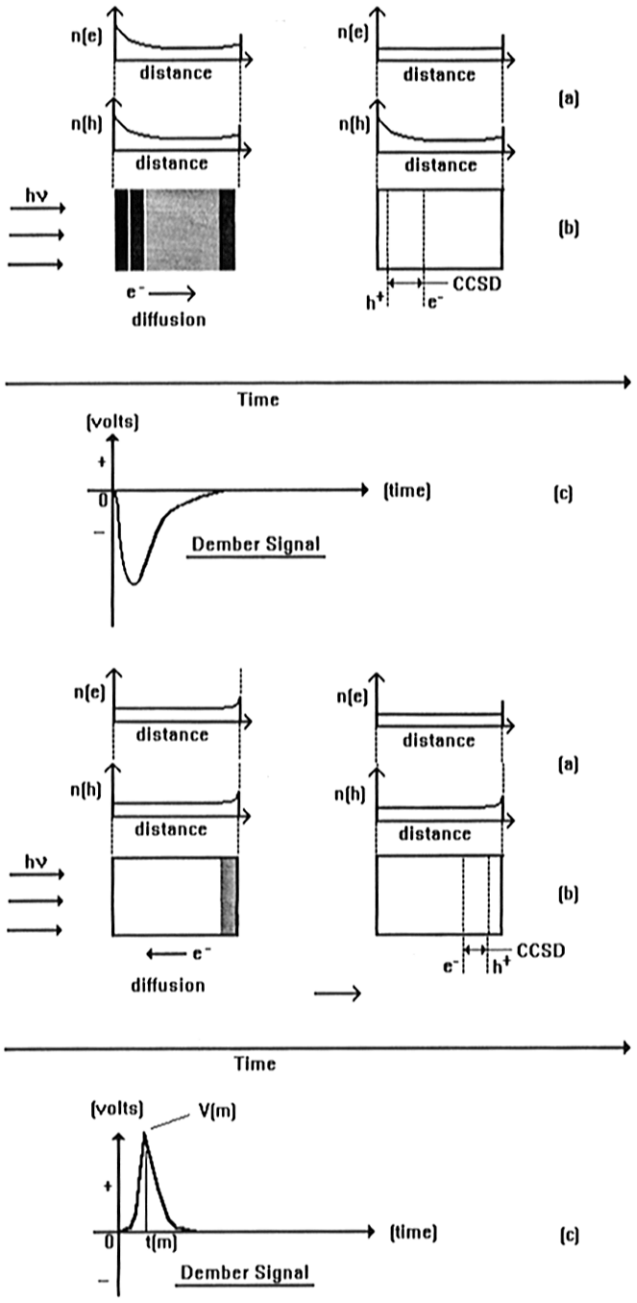

Figure 3. Photoinduced carrier distribution in a thin film or a small particle: (a, top) strongly absorbed light pulse; (b, bottom) weakly absorbed light pulse. Concentration distributions are shown immediately after pulse on left and some time *t* later on right depicting flattening of electron gradient by diffusion. Here, electron mobility is greater than hole mobility. Also shown is separation length of center of mass of charge. Time-resolved Dember signal is shown below charge distributions.

of the surrounding media, and (iv) angle of incidence of the excitation light pulse with the inside back surface of a homogeneous photoconductor or the "effective" light-absorbing unit of a coating consisting of particulate aggregates.

For strongly absorbed light Beer's law is applicable,

$$I_B/I_F = (e^{-kd})_{\text{absorbance}} \tag{3}$$

where I_B is the light intensity at the inside back surface of the sample, I_F is the light intensity on the front surface of the sample, k is the absorption coefficient of the sample at the wavelength of excitation, and d is the sample thickness for a homogeneous sample or the effective particle size for a coating comprising

aggregated particles. As the wavelength of the excitation light is increased, the long wavelength absorption edge is approached, and constructive interference between incident and reflected light at the inside back surface of the sample must be considered in assessing the region within the sample where the light intensity is highest. Since this is also the region where the highest concentration of charge carriers is generated, the location of this region determines the vectorial direction of the diffusion currents. As discussed and verified experimentally in refs 17, 19−22, 24, 26, and 27 when Beer's law absorbance at the front surface is approximately equal to the constructive interference effect at the inside back surface, there will be no observable diffusion currents. This condition has been expressed as

$$\left(\frac{I_B}{I_F}\right)_{\text{absorbance}}\left(\frac{I_B}{I_F}\right)_{\text{interference}} \approx 1 \qquad (4)$$

Introduction of eq 3, the expression for Beer's law absorbance into eq 4 and substituting γ for (I_B/I_F) gives eq 5.

$$(e^{-kd})_{\text{absorbance}}(\gamma)_{\text{interference}} \approx 1 \qquad (5)$$

Thus, for a sample of given thickness d, the absorption coefficient k at which sign reversal is expected is approximated by eq 6.

$$k \approx (\ln \gamma)/d \qquad (6)$$

The dependence of $(\gamma)_{\text{interference}}$ on the angle on incidence of the photon flux with the front surface of the sample, ϕ_0, as it relates to the angle of incidence of the light on the inside back surface of the photoconductor ϕ' and the angle of refraction ϕ out of the back surface of the photoconductor into the surrounding media can be assessed by application of the Fresnel equations and of Snell's law.

The relationship of $(\gamma)_{\text{interference}}$ to ϕ' , using the Fresnel equations, is given in eq 7,

$$(\gamma)_{\text{interference}} = \frac{(1+R_p)^2 \sin\phi' + (1-R_p)^2 \cos^2\phi' + (1+R_s)^2}{2+(R_p)^2+(R_s)^2} \qquad (7)$$

where R_s and R_p are the perpendicular and parallel reflected electric vectors at the inside back surface of the sample, respectively.

Application of Snell's law allows evaluation of ϕ' for various values of the angle of incidence of the photon flux on the sample ϕ_0, using the known refractive indexes of the photoconducting sample and the surrounding media. The calculated values of $(\gamma)_{\text{interference}}$ vs ϕ_0 for a 0.1 cm thick AgCl crystal were found to be in good agreement with experimental TRPC determinations especially designed to allow rotation of the AgCl crystal to various angles ϕ_0. In other respects this TRPC apparatus was similar to that shown in Figures 1 and 2.

A positive TRPC signal could also result in strongly absorbed light (front surface light absorption) if the photon flux opposes a sufficiently large preexposure-induced potential gradient within the film, in which case the observed signal is the vectorial sum of these diffusion and drift components and can no longer be viewed as a pure Dember effect.

As will be discussed in further detail in the Results and Discussion section, in the case of the lightly sintered nanostructured TiO_2 films coated directly on glass, as shown in Figures 4 and 5, when using 337 nm pulsed excitation the effective particle size of the sintered aggregates appears to be sufficiently large to yield TRPC signals of negative polarity regardless of which surface of the TiO_2 is facing toward the incident light and whether or not continuous wave (CW) xenon excitation is employed concurrent with the 337 nm pulsed laser excitation. Assuming that the photoelectrons generated in TiO_2 have higher velocity than the photoholes, these results indicate that more light is being absorbed close to the TiO_2 surface upon which the light is directly incident, as compared to the back surface facing away from the incident light. On this basis the TRPC sign reversals of Figures 6 and 7, which are observed to occur with the SnO_2(F)/TiO_2 samples when the orientation of the samples are reversed with respect to the surface upon which the pulsed or pulsed plus CW light is incident, are attributed to the contact potential across the SnO_2(F)/TiO_2 junction, which in all cases directs photoelectron currents toward the SnO_2(F) phase. Back surface light intensity reinforcement, resulting from constructive interference of the incident and reflected light at the inside back surface, is thereby shown not to be the cause of the observed TRPC sign reversals of the SnO_2(F)/TiO_2 heterojunctions investigated.

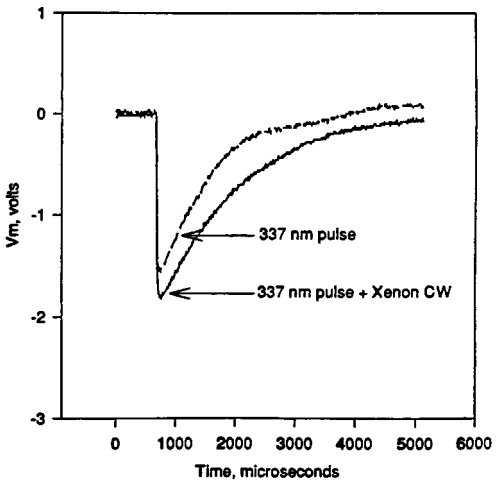

Figure 4. TRPC wave forms for nanocrystalline TiO_2 coated on glass support. Excitation with (a) 337 nm laser pulse and (b) 337 nm laser pulse + CW xenon lamp. Glass surface is facing incident light.

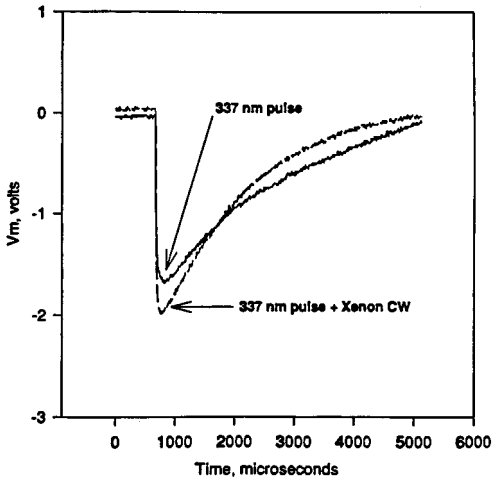

Figure 5. TRPC wave forms for nanocrystalline TiO_2 coated on glass support. Excitation with (a) 337 nm laser pulse and (b) 337 nm laser pulse + CW xenon lamp. TiO_2 surface is facing incident light.

Since TRPC measurements require neither direct electrical contact with the sample being investigated nor an externally applied field, it may be described as analogous to a noncontact zero field time-of-flight technique or a noncontact time-resolved surface photovoltage measurement.[17,19−22] In this respect it shares certain features in common with time-resolved microwave

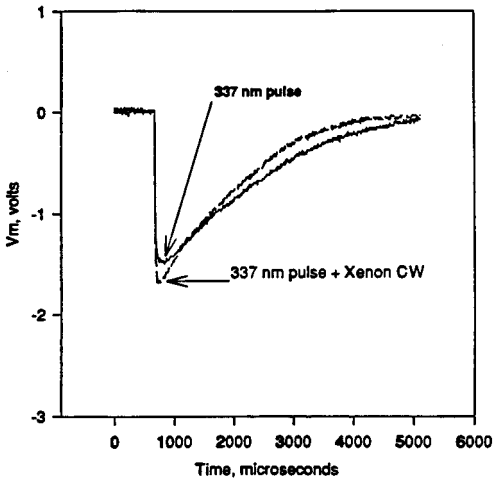

Figure 6. TRPC wave forms for nanocrystalline TiO_2 coated on SnO_2(F)-coated glass support. Excitation with (a) 337 nm laser pulse and (b) 337 nm laser pulse + CW xenon lamp. TiO_2 surface is facing incident light.

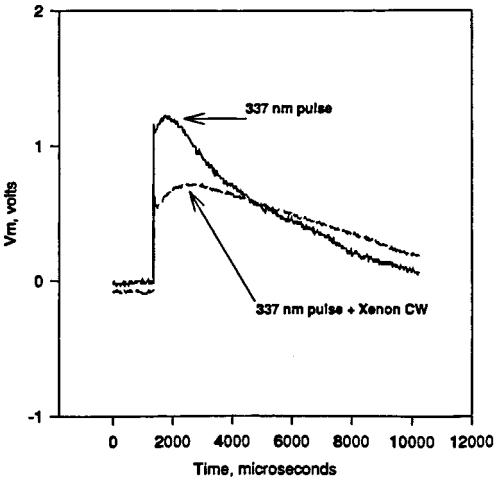

Figure 7. TRPC wave forms for nanocrystalline TiO_2 coated on SnO_2(F)-coated glass support. Excitation with (a) 337 nm laser pulse and (b) 337 nm laser pulse + CW xenon lamp. Glass surface is facing incident light.

photoconductivity (TRMC), measuring related but different parameters.[17] TRPC may be considered a direct probe of charge carrier separation dynamics, while TRMC is a measure of the dynamics of population and decay of photoelectrons into and out of the conduction band.

Experimental Section

Sample Preparation. Films of colloidal nanocrystalline TiO_2 (anatase) were prepared by spreading a colloidal suspension of anatase particles (10−100 nm) to a thickness of 10 μm on glass sheets, with and without a conductive but transparent coating of fluorine-doped SnO_2. The colloidal suspension was prepared following the procedure of O'Regan and Grätzel,[28] but autoclaved at 250 °C to allow aggregates of ∼100 nm diameter to form. The wet films were then lightly sintered in air at 450 °C for 15 min, forming films of ∼8 μm thickness for the samples of the present investigation.

TRPC Measurements. Sample excitation was by single-pulse 10 ns duration, 337 nm light supplied by a Molectron Model UV-24 nitrogen laser, with and without CW xenon illumination. The laser pulse energy was 9 mJ/pulse, and the CW illumination from a Varian 150 W xenon lamp operated at 6 A filament current at a distance from the sample of 18 in. The illumination was performed as a function of sample orientation with respect to the surface of the films facing the incident light. (When pulsed light of other wavelengths are required, the Molectron Model UV-24 nitrogen laser is used to pump a Molectron DL-II tunable dye laser, as shown in Figure 1.)

The experimental configuration is shown in Figure 1. The apparatus consists of a parallel plate spring-loaded sample cell, with blocking contacts. The glass plates supporting the films were loaded into the sample chamber oriented with the illumination directly incident either on the TiO_2 film or on the glass substrate. The chamber was at ambient conditions of temperature and pressure. Illumination consisted of the laser pulse with and without simultaneous CW xenon irradiation. The TRPC wave forms displayed in Figures 4−7 are the averaged results of 10 determinations taken at 1 s intervals between the 10 ns duration 337 nm laser pulses. Individual determinations were randomly reproducible to within 10%, with no discernible trend based on sequential order of the individual measurements.

Results and Discussion

Typical TRPC transient wave forms are shown in Figure 4. *Vm* represents the time-resolved instrumental response to the photoinduced charge carrier separation and recombination within the nanoporous TiO_2 coating. The figure shows wave forms generated by the 337 nm pulsed laser, with and without the CW xenon source, demonstrating an enhancement of the signal with CW illumination. In this case, the sample consists of the nanoporous anatase film coated on an ordinary glass substrate. Light is directly incident on the film. In Figure 5, the sample is the same but its configuration is reversed; that is, light is now incident on the glass. The TRPC signals display essentially the same characteristics, except for a slower decay in the case of the laser pulse without the CW source.

In control experiments, without the TiO_2, using the SnO_2/(F) transparent conducting coating on a glass substrate, there was no measurable TRPC response. Similarly, the glass substrate alone in the absence of SnO_2(F) did not yield a measurable signal.

For the nanoporous TiO_2 film deposits on SnO_2(F)-coated glass, reversal of sample orientation with respect to the photon flux caused a polarity reversal of the TRPC signal. Direct illumination of the TiO_2 surface yielded transients virtually identical to those obtained with TiO_2 films on nonconducting glass, as exemplified in Figure 6. When exposure is through the SnO_2/TiO_2 junction, the TRPC signal exhibits a change of sign, as shown in Figure 7. In addition, it is seen in Figure 7 that the CW illumination causes a marked decrease in |Vm|. Note that the decay time is essentially doubled as well.

The effect of the CW illumination, as shown in Figures 4−6, is to increase |*Vm*|. This can be interpreted as an enhanced mean charge carrier separation distance, CCSD, (i) by decrease in intraparticle band bending at junctions between large particles formed during the sintering process, implying that upward bandbending occurs at these boundaries which would confine photogenerated carriers and increase the chances for recombination; or (ii) due to a trap-filling process (which could also decrease band bending in situations where the filled traps have the net effect of raising the Fermi level). The sign reversal of the TRPC signal upon illumination through the glass support of the glass/SnO_2(F)/TiO_2 structure demonstrates that, for TiO_2 films in contact with the SnO_2(F) conducting glass, the photoelectrons flow toward the SnO_2(F), independent of sample orientation with respect to photon flux. This strongly indicates the presence of a built-in contact potential with electric field

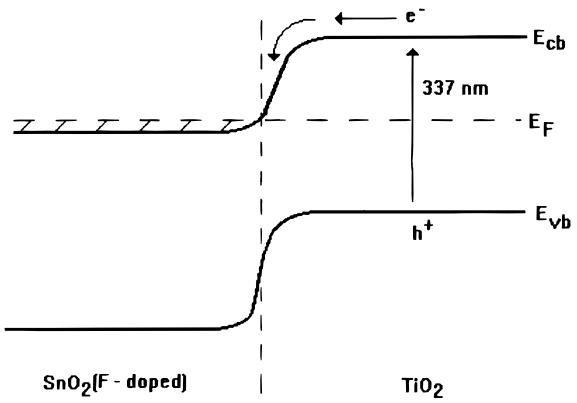

Figure 8. Energy band diagram for bulk TiO_2 coated on SnO_2 degenerately doped with fluorine.

driving electrons toward the $SnO_2(F)/TiO_2$ junction. Further evidence for the existence of the contact potential is borne out of the effect of CW irradiation, seen in Figure 7, in that |Vm| is decreased markedly when the CW xenon lamp is employed. Here, it is believed that the xenon illumination collapses the band bending at the junction by driving the bands toward a flat band condition, causing an enhancement of the recombination kinetics of the electron−hole pairs generated during the light pulse. A simple band diagram of the SnO_2/TiO_2 junction is proposed in Figure 8, based on two wide gap semiconductors ($E_g = 3.2$ eV for anatase,[29] $E_g = 3.8$ eV for SnO_2[30]), where the SnO_2 is degenerately doped and the TiO_2 virtually intrinsic. Equilibration of the Fermi levels would create a depletion layer in the SnO_2. Photoelectrons generated furthest away from the SnO_2/TiO_2 junction are driven toward it mainly by diffusion. Hagfeldt *et al.*[15] have shown enhanced quantum efficiency in nanocrystalline anatase photoelectrodes when illumination was through a SnO_2 transparent electrode, compared to illumination at the front surface of the TiO_2 film. Similar results were also reported with front/back illumination of TiO_2/CdSe nanocrystalline films operated as photoelectrodes.[31] In these studies, effective electron−hole pair separation was enhanced at the back contact, but it was not clear whether this was caused by downward band bending at the heterojunction enhanced by positive applied voltage or by emptying of deep traps in the vicinity of the contact caused by the positive polarization of the SnO_2 electrode.

The spontaneously formed field at the $SnO_2(F)/TiO_2$ junction certainly does not appear to aid the separation of electron−hole pairs when exposure is directed on the nanocrystalline TiO_2—not through the glass/SnO_2(F) interface first—since the magnitudes of the photocharge responses, in both the presence and absence of $SnO_2(F)$, are about the same, as seen by comparison of Figures 4 and 6. It is especially significant to note that when exposure is through the $SnO_2(F)$ transparent electrode, the situation is very different, as seen in Figure 7. Here, due to the high absorptivity of the 337 nm light by TiO_2, the highest concentration of photoinduced charge carriers in the TiO_2 is adjacent to the contact potential induced, positively charged field in the $SnO_2(F)$ deposit. This initiates drift of photoelectrons toward the $SnO_2(F)$, resulting in net vectorial flow of photoelectrons in a direction that opposes the diffusion current. Diffusion, however, dominates the transient photoelectron current in TiO_2 films coated on ordinary glass, where the drift component is small, as seen in Figures 4 and 5, and the effects of CW illumination are to cause relatively small increases in the TRPC signal amplitudes, possibly due to reduction in interparticle band bending. A similar explanation is believed applicable to the glass/$SnO_2(F)/TiO_2$ sample when light is incident directly on the TiO_2, as seen in Figure 6.

The field exerted by the $SnO_2(F)$ electrode appears to be effective over relatively short distances. The extinction coefficient of the 337 nm laser pulse is estimated to be $\sim$5500 cm^{-1} in the TiO_2 film;[15] therefore, over 90% of the light would be absorbed within the first 4 μm. Thus, the extent of the depletion width emanating from the back $SnO_2(F)$ contact, when present, is restricted to much less than 4 μm, and electron−hole pairs generated in the top half of the film do not experience a drift field in the case of front side illumination, since a drift field would be expected to augment the TRPC signal, and this is not observed in Figure 6. Hagfeldt and co-workers[15] have estimated the effective ambipolar charge separation in films similar to those used in the present study to be 0.5 μm by applying the analysis of Lindquist *et al.*[32] based on the Gärtner−Butler model of space charge formation at the semiconductor−electrolyte junction. Thus, essentially all of the carriers are generated in the top half of the film with front-side illumination and, because of the relatively small charge separation distance of 0.5 μm, are confined to that region. No difference is observed in TRPC maxima between films coated on glass or on $SnO_2(F)$ electrodes with front-side illumination, supporting the view that in the latter systems the top half of the films are essentially field-free, except for localized interparticle band bending effects.

Conclusion

It has been demonstrated that TRPC measurements are sensitive to potential gradients existing at the junction between $SnO_2(F)$ and nanocrystalline colloidal films of TiO_2. As a contactless technique, TRPC yields relatively unambiguous results, since other than the comparatively small TiO_2 interparticle band bending, the only contact potential present in the samples is that due to the $SnO_2(F)/TiO_2$ junction. The strongly absorbed 337 nm laser light incident on the front TiO_2 component of the 8 μm thick films is primarily absorbed within the top 4 μm, as indicated by the negative polarity of the TRPC signal. No difference is seen in the TRPC signal for films prepared on ordinary glass supports or those prepared on $SnO_2(F)$-coated glass, providing evidence that the effective charge separation distance is within the zone of light absorption, <4 μm. Under these conditions diffusion currents are dominant. Simultaneous illumination with a 337 nm laser pulse and CW xenon light causes a slight enhancement of the TRPC signal, Vm, as compared to 337 nm laser pulse excitation alone (i) in TiO_2 films coated directly on glass (no $SnO_2(F)$) independent of sample orientation with respect to photoflux (Figures 4 and 5) and (ii) with $SnO_2(F)/TiO_2$ films when the TiO_2 surface was exposed to the pulsed laser photon flux (Figure 6). This can be interpreted as the result of either (i) collapsing interparticle potential barriers (decreased band bending) or (ii) a trap-filling effect of the CW light, which may extend the apparent lifetime of the photoelectrons generated by the laser pulse.

However, when the $SnO_2(F)/TiO_2$ junction is illuminated through the $SnO_2(F)$ transparent electrode (Figure 7), the TRPC signal polarity is inverted, indicating a reversal of the vectorial direction of the net electron transport with respect to the case where light is incident on the front surface of the TiO_2 film (Figure 6). These results imply the presence of a spontaneously formed potential gradient across the $SnO_2(F)/TiO_2$ heterojunction due to Fermi level equilibration prior to light excitation, with the direction of the electric field favoring electron transport toward the $SnO_2(F)$ electrode for collection. The presence of a spontaneous electric field is further evidenced by the reduction of the TRPC signal amplitude, |Vm|, when CW light is

simultaneously incident with the laser pulse (Figure 7). We interpret this to mean that the CW light collapses the electric field by reducing the space charge present at the $SnO_2(F)/TiO_2$ junction, thereby diminishing the charge carrier separation distance between photoelectrons and photoholes and enhancing recombination. This implies that with the glass/$SnO_2(F)/TiO_2$ sample drift currents are dominant when the 337 nm laser pulse is directly incident on the glass surface.

In this sense, experimental observations of the present investigation are in agreement with earlier studies demonstrating more efficient photoelectron collection for exposure incident on the $SnO_2(F)$ component of the $SnO_2(F)/TiO_2$ heterojunction.[8,15] The essential departure is the inclusion of consideration of a drift induced photoelectron current which opposes diffusion toward the interior of the TiO_2 and results in a net vectorial flow toward the $SnO_2(F)/TiO_2$ interface (positive TRPC signal polarity).

Acknowledgment. We thank Professor Michael Grätzel for generously supplying the TiO_2 films used in this investigation. Support for research performed at Boston University was provided in part by the National Science Foundation, under Grant CTS-9208926, and is gratefully acknowledged.

References and Notes

(1) Nazeeruddin, M. K.; Rodicio, I.; Humphrey-Baker, R.; Müller, E.; Liska, P.; Vlachopoulos, N.; Grätzel, M. *J. Am. Chem. Soc*. **1993**, *115*, 6382.

(2) Hagfeldt, A.; Vlachopoulos, N.; Grätzel, M. *J. Electrochem. Soc.*, in press.

(3) Lin, H. M.; Hsu, C. M.; Yang, H. Y.; Leeb, P. Y.; Yang, C. C. *Sens. Actuators, B* **1994**, *22*, 63.

(4) Hoyer, P.; Eichberger, R.; Weller, H. *Ber. Bunsen-Ges. Phys. Chem*. **1993**, *97*, 630.

(5) Kavan, L.; Stoto, T.; Grätzel, M.; Fitzmaurice, D.; Shklover, V. *J. Phys. Chem*. **1993**, *97*, 9493.

(6) O'Regan, B.; Moser, J.; Anderson, M.; Grätzel, M. *J. Phys. Chem*. **1990**, *94*, 8720.

(7) Schwartzburg, K.; Willig, F. *Appl. Phys. Lett*. **1991**, *58*, 2520.

(8) Sodergren, S.; Hagfeldt, A.; Olsson, J.; Lindquist, S.-E. *J. Phys. Chem*. **1994**, *98*, 5552.

(9) Könenkamp, R.; Henninger, R.; Hoyer, P. *J. Phys. Chem*. **1993**, *97*, 7328.

(10) Könenkamp, R.; Henninger, R. *Appl. Phys. A* **1994**, *58*, 87.

(11) Rothenberger, G.; Fitzmaurice, D.; Grätzel, M. *J. Phys. Chem*. **1992**, *96*, 5983.

(12) Björkstén, U.; Moser, J.; Grätzel, M. *Chem. Mater*. **1994**, *6*, 858.

(13) Kay, A.; Humphry-Baker, R., Grätzel, M. *J. Phys. Chem*. **1994**, *98*, 952.

(14) Hoyer, P.; Eichberger, R.; Weller, H. Ber. *Bunsen-Ges. Phys. Chem*. **1993**, *97*, 630.

(15) Hagfeldt, A.; Björkstén, U.; Lindquist, S.-E. *Sol. Energy Mater. Sol. Cells* **1992**, *27*, 293.

(16) Castellano, F. N.; Stipkala, J. M.; Friedman, L. A.; Meyer, G. J. *Chem. Mater*. **1994**, *6*, 2123.

(17) Levy, B. Photocatalytic and photographic heterojunctions. In *Photochemical Conversion and Storage of Solar Energy*; El Pelizzetti, Schiavello, M., Eds.; Kluwer Academic: Dordrecht, 1991; pp 357−392.

(18) Hodes, G.; Howell, I. D. J.; Peter, L. M. *J. Electrochem. Soc.* **1992**, *139*, 3136.

(19) Sadeghi, M.; Liu, W.; Zhang, T.-G.; Stavropoulos, P.; Levy, B. The Role of Photo-Induced Charge Carrier Separation Distance in Heterogeneous Photocatalysis: Oxidative Degradation of CH_3OH Vapor in Contact with Pt/TiO_2 and Cofumed $TiO_2-Fe_2O_3$. *J. Phys. Chem.* **1996**, *100*, 19466.

(20) Levy, B. *Photogr. Sci. Eng*. **1971**, *15*, 279.

(21) Levy, B.; Zhang, T.-G. *Bulg. Chem. Commun.* **1993**, *26* (3/4), 412.

(22) Zou, C.-F.; Sahyun, M. R. V.; Muller, M. E.; Levy, B.; Zhang, T.-G. *J. Imaging Sci. Technol*. **1995**, *29*, 106.

(23) Tiedje, T. Information about Band Tail States from Time-of-Flight Experiments. In *Semiconductors and Semimetals*; Pankove, J. I., Ed.; Academic Press: New York, **1984**; Vol. 21, Part C, pp 207−238.

(24) Dickson, C. R.; Levy, B. *Photogr. Sci. Eng*. **1974**, *18*, 524. Levy, B. Heterojunctions in Imaging and Photoconducting Catalytic Systems. In *Symposium on Electronic and Ionic Properties of Silver Halides—Common Trends with Photocatalysis*; Levy, B., Ed.; The Society for Imaging Science and Technology: Springfield, VA, 1991; pp 189−197.

(25) Wang, Y.; Heron, N. *J. Phys. Chem*. **1991**, *95*, 525.

(26) Levy, B.; Lindsey, M.; Dickson, C. R. *Photogr. Sci. Eng*. **1973**, *17*, 115.

(27) Levy, B.; Dickson, C. R. *Photogr. Sci. Eng*. **1975**, *19*, 79.

(28) O'Regan, B.; Grätzel, M. *Nature* **1991**, *353*, 737.

(29) Tang, H.; Prasad, K.; Sanginès, R.; Schmid, P. E.; Lévy, F. *J. Appl. Phys*. **1994**, *75*, 2042.

(30) Grätzel, M. *Heterogeneous Photochemical Electron Transfer*; CRC Press: Boca Raton, FL, 1989.

(31) Liu, D.; Kamat, P. V. *J. Phys. Chem*. **1993**, *97*, 10769.

(32) Lindquist, S.-E.; Finnström, B.; Tegnér, L. *J. Electrochem. Soc*. **1983**, *130*, 351.